

Continuing Colorado plateau uplift by delamination-style convective lithospheric downwelling

A. Levander¹, B. Schmandt², M. S. Miller³, K. Liu¹, K. E. Karlstrom⁴, R. S. Crow⁴, C.-T. A. Lee¹ & E. D. Humphreys²

The Colorado plateau is a large, tectonically intact, physiographic province in the southwestern North American Cordillera that stands at ~1,800–2,000 m elevation and has long been thought to be in isostatic equilibrium¹. The origin of these high elevations is unclear because unlike the surrounding provinces, which have undergone significant Cretaceous–Palaeogene compressional deformation followed by Neogene extensional deformation, the Colorado plateau is largely internally undeformed. Here we combine new seismic tomography² and receiver function images to resolve a vertical high-seismic-velocity anomaly beneath the west-central plateau that extends more than 200 km in depth. The upper surface of this anomaly is seismically defined by a dipping interface extending from the lower crust to depths of 70–90 km. The base of the continental crust above the anomaly has a similar shape, with an elevated Moho. We interpret these seismic structures as a continuing regional, delamination-style foundering of lower crust and continental lithosphere. This implies that Pliocene (2.6–5.3 Myr ago) uplift of the plateau and the magmatism on its margins are intimately tied to continuing deep lithospheric processes. Petrologic and geochemical observations indicate that late Cretaceous–Palaeogene (~90–40 Myr ago) low-angle subduction hydrated and probably weakened much of the Proterozoic tectospheric mantle^{3–5} beneath the Colorado plateau. We suggest that mid-Cenozoic (~35–25 Myr ago) to Recent magmatic infiltration subsequently imparted negative compositional buoyancy to the base and sides of the Colorado plateau upper mantle, triggering downwelling. The patterns of magmatic activity suggest that previous such events have progressively removed the Colorado plateau lithosphere inward from its margins⁶, and have driven uplift. Using Grand Canyon incision rates^{7,8} and Pliocene basaltic volcanism patterns, we suggest that this particular event has been active over the past ~6 Myr.

Unlike the basement-involved Laramide uplifts of the Rocky Mountains (~2,200 m elevation) and the 100% extension of the Basin and Range (at 1,000–1,600 m elevation) since the mid-Cenozoic, the Colorado plateau (Fig. 1) has experienced only mild internal deformation (~1% shortening), manifested as long-wavelength monoclines. Xenolith data indicate that central Colorado plateau mantle consisted of Proterozoic (~1.7–2.0 Gyr old) North American tectospheric mantle extending to 120 km depth as recently as 20–40 Myr ago^{4,9}. In the Late Miocene and Pliocene, the western and southern peripheries of the plateau were invaded by basaltic magmas⁶ whose Nd and Sr isotopes indicate an increasingly undepleted mantle source^{7,10}.

The timing of both Colorado plateau uplift and formation of the Grand Canyon remain unresolved, with various lines of evidence suggesting episodes of uplift in the Laramide^{11,12}, mid-Cenozoic^{3,13} and late Cenozoic^{8,14,15}. The cumulative uplift history probably reflects lithospheric preconditioning from hydration of the North American lithosphere during Farallon plate flat-slab subduction that weakened the overriding plate, possibly removing any North American lithosphere deeper than 120–150 km, and cooling the remainder from

below. Models for late Cenozoic steady magmatic invasion of the northwestern and southern margins towards the core of the Colorado plateau and the related plateau uplift are attributed to

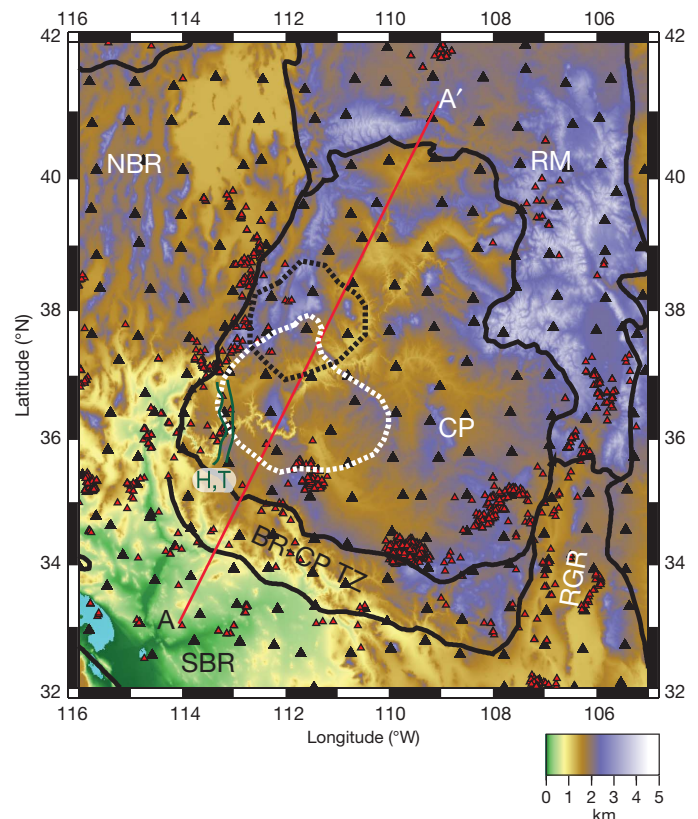


Figure 1 | Elevation map of the Colorado plateau. The map shows topography, in km, of the Colorado plateau and surrounding tectonic/physiographic provinces, province boundaries (black lines), and the locations of approximately 220 seismograph stations. CP, Colorado plateau; NBR, northern Basin and Range; SBR, southern Basin and Range; RGR, Rio Grande rift; RM, Rocky Mountains; BR-CP TZ, Basin and Range–Colorado Plateau transition zone. H, Hurricane fault; T, Toroweap fault. Black triangles, USArray Transportable Array and other broadband seismograph stations used in the seismic analysis; red triangles, volcanic rocks less than 10 Myr old. Profile AA' is the location of the cross-sections in Fig. 3. White dashed line, region of lower-crustal delamination and crustal thinning, with the western edge coinciding with active normal faults (blue lines) that mark ~100 m Myr⁻¹ differential uplift of the Colorado plateau relative to BR. Young volcanics ring the delamination region. Black dashed line, outline of the downwelling body at 200 km depth estimated from the body wave tomography (Figs 3 and 4). The Grand Canyon is centred on the delamination region, suggesting that the downwelling influenced re-routing of Rocky Mountain and Colorado plateau headwaters into a through-going Colorado River that carved the Grand Canyon in the last 5–6 Myr (ref. 8).

¹Earth Science Department, Rice University, Houston, Texas 77005-1892, USA. ²Department of Geological Sciences, University of Oregon, Eugene, Oregon 97403, USA. ³Department of Earth Sciences, University of Southern California, Los Angeles, California 90089-0740, USA. ⁴Department of Earth and Planetary Sciences, University of New Mexico, Albuquerque, New Mexico 87131, USA.

conductive heating and thermal expansion⁶ and small-scale convective removal of Colorado plateau lithospheric mantle⁸.

Here we review seismic evidence that suggests how asthenosphere-derived melts are invading the Colorado plateau, and present evidence that suggests how these melts destabilize continental lithosphere and drive uplift. Previous active and passive seismic probes image shallow low-velocity zones (LVZ) under the southwestern Colorado plateau at 40–50 km depth (P-wave velocity $v_p \approx 7.5 \text{ km s}^{-1}$) and under its eastern margin at 50–75 km depth ($v_p \approx 7.6\text{--}7.7 \text{ km s}^{-1}$), with both LVZs lying beneath thin lithospheric lids with $v_p \approx 7.9 \text{ km s}^{-1}$ (refs 16, 17). Recent USArray Transportable Array P_n tomography measured upper-mantle velocities of $\sim 8.0 \text{ km s}^{-1}$ in the centre of the Colorado plateau, with 7.9 km s^{-1} and lower velocities along its western and southern peripheries¹⁸.

We use PdS and SdP receiver functions to determine discontinuity structure beneath the Colorado plateau and its surroundings, and finite-frequency P and S body wave and Rayleigh wave tomography to construct three-dimensional models of v_p , v_s and v_p/v_s under the plateau¹⁹. The data for all these studies were recorded by the Transportable Array, other portable array experiments, and regional networks (Fig 1). The velocity model used for depth-positioning the receiver functions was constructed by smoothly blending Crust2.0

(ref. 20) with the upper-mantle P_n (ref. 18) and deeper-mantle teleseismic tomography¹⁹ models.

Finite-frequency body-wave tomography finds low v_p , very low v_s and high v_p/v_s at $\sim 60\text{--}200 \text{ km}$ beneath the periphery of the Colorado plateau, forming a ring around its eastern, southern and northwestern edges, surrounding a higher-velocity, lower- v_p/v_s core (Fig. 2). Rayleigh wave tomography images a similar pattern of low shear velocities under the edges of the Colorado plateau, but with somewhat greater vertical resolution. Figure 2 compares the v_p and v_p/v_s anomalies (perturbations) and Rayleigh wave shear velocities at 80 km depth, and the depth of the lithosphere–asthenosphere boundary (LAB) from receiver functions and the Rayleigh wave v_s model. We interpret the low-velocity ring as low-melt-fraction asthenosphere surrounding the Colorado plateau lithospheric core.

Along profile AA' (Fig. 1), the receiver function discontinuity structures and v_p and v_s tomography images show a set of structures suggestive of lower-crust and upper-mantle delamination (Fig. 3). The PdS receiver functions show a clearly defined Moho at 35–40 km and a bright sub-Moho event dipping $\sim 10^\circ$ northeast from ~ 50 to 90 km depth, between 35.5° and 38.0° N . Above the dipping event, a weaker event that we interpret as a 'new' Moho is elevated by approximately the thickness of the dipping event (10 km) over the same $\sim 280 \text{ km}$

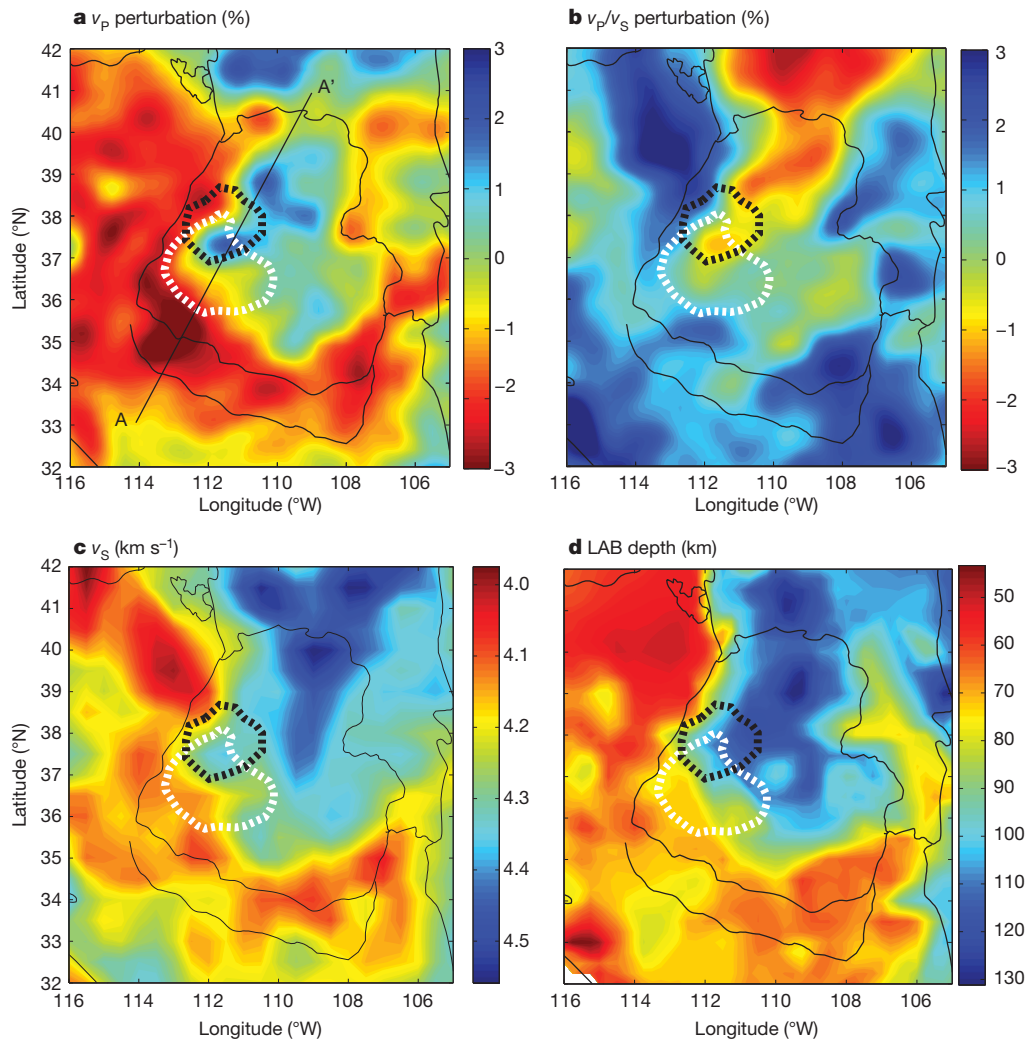


Figure 2 | Seismic velocity measurements at 80 km depth, and LAB depth, as measured with different seismic probes. **a**, **b**, Perturbations of v_p (**a**) and v_p/v_s (**b**) at 80 km depth determined by teleseismic body wave tomography. **c**, Shear velocity at 80 km depth measured by Rayleigh wave tomography. **d**, LAB depth determined from the receiver functions and the maximum negative vertical gradients in v_s as determined from the Rayleigh wave inversions. The Colorado

plateau is partially encircled by low v_p and v_s , and high v_p/v_s , suggestive of low-volume partial melt. The LAB is at shallow depths in the regions of low v_p and v_s , and high v_p/v_s , and deepens rapidly to the north under the central Colorado plateau and the Rocky Mountains. The locations of the crustal delamination region and the outline of the downwelling are shown as in Fig. 1.

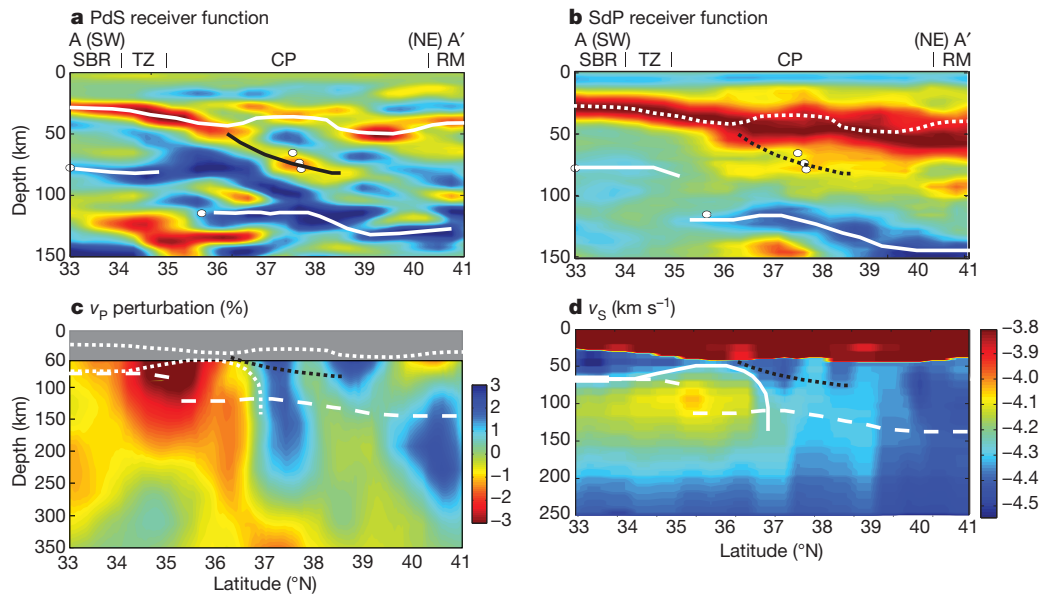


Figure 3 | Receiver function and seismic velocity cross-sections through the downwelling region. In all panels, the solid lines indicate surfaces chosen on that section, dashed lines are superimposed surfaces picked from the other sections. **a, b**, PdS (**a**) and SdP (**b**) receiver function sections along AA' (Fig. 1). The PdS section shows a bifurcation in the Moho (upper white line) at ~36° N, with one branch shoaling to ~30 km and the other (black line) descending to 80–90 km. A negative polarity signal appears above the positive dipping event. At the same depths, the SdP receiver function shows a broadened positive lobe, the result of interference of two long period (5 s) pulses (Supplementary Information). The estimated melting depths of basalts along this profile are shown as white circles, and appear on either side of the deeper (black) surface.

width. These two P to S conversions are apparent on a large number of stations (Supplementary Fig. 1a, b). The pattern suggests to us that the dipping structure once fitted in the Moho notch above it; this suggestion is supported by our examination of the dipping event and the shallow Moho in three dimensions (Supplementary Fig. 2), where we find approximately the same volume in the top of the dipping event as that beneath the elevated Moho and the surrounding Moho. We suggest that the lowermost crust and uppermost mantle are delaminating from the base of the Colorado plateau, as suggested previously²¹, and as modelled in some two-dimensional geodynamic models^{21,22}.

Although this dipping structure is not as clear in the SdP receiver functions, the section shows complications beneath the Moho in the same places as the dipping event in the PdS receiver functions throughout the region outlined in Figs 1 and 2. We note that the resolution of SdP receiver functions is ~5 times coarser than that of PdS owing to differences in frequency content, and the blurred SdP image is expected from the lower frequency SdP receiver functions (Supplementary Fig. 3).

Directly beneath the dipping sub-Moho structure in the receiver function image, body wave tomography shows an elongate high-velocity body extending from 60 to greater than 200 km depth, with necking at about 100 km depth. The body wave tomography also shows high velocities and low v_p/v_s beneath the core of the Colorado plateau, typical of cratonic mantle lithosphere (Fig. 2). The Rayleigh wave v_s tomography model shows a strong LVZ ~100 km to the southwest of the drip region that changes to a pattern of intermediate and high velocities consistent with the receiver function sections. To the north, Rayleigh wave v_s becomes uniformly faster beneath the Colorado plateau core. Similar patterns appear in cross-sections taken at different azimuths through this area (Supplementary Fig. 4). Thus, using multiple seismic data analyses and techniques we identify this anomalous region (Fig. 1) as a currently occurring delamination-style convective downwelling, the causes of which we describe below.

The LAB is shown by the two deeper solid white lines in **a** and the two solid white lines in **b, c**. The v_p perturbation image shows a high-velocity downwelling that extends to >200 km depth, with necking at about 100 km depth. Note the vertical scale change. The downwelling is directly below the Moho bifurcation shown in **a**. **d**, v_s from Rayleigh wave tomography shows a pronounced upper-mantle LVZ in the southwestern part of the line to 112° W. Northeast of this, at ~100 km depth, v_s increases relative to the south. The LAB determined from the Rayleigh wave tomography is shown as a solid white line in **d** and as a short-dashed white line in **c**. The LAB from the SdP cross-section is shown as a long-dashed white line in **c** and **d**.

The Moho and the deeper surfaces suggest that the currently active lithospheric foundering has propagated northeast to southwest, consistent with Grand Canyon uplift rates since 6 Myr ago inferred by its incision history, which indicates more rapid uplift in the eastern canyon (175–250 m Myr⁻¹) than in the western canyon (50–80 m Myr⁻¹)⁸. Simple thermally based isostatic calculations on endmember models suggest that ~400–800 m of uplift would be possible if the entire Colorado plateau lithosphere were to be instantly replaced with asthenosphere, either with or without asthenospheric replacement of 10 km of lower crust (Supplementary Fig. 5). This estimated range is consistent with geologic evidence for uplift of the western Colorado plateau since 6 Myr ago. The amount of uplift is proportional to the ratio of the density of Colorado plateau lithosphere to that of asthenosphere. We describe below a means by which the density of the Colorado plateau lithosphere could have been increased.

Commonly suggested driving mechanisms for lithospheric foundering are: convective instability, with the lithosphere replaced by asthenosphere following orogenic thickening or some other perturbation of thermal boundary layers^{21,23,24}, development of eclogitic roots by the generation of mafic cumulates and restites during arc magmatism^{25,26}, and erosion of the lithosphere by a flat-subducting slab^{27,28}. However, no tectonic processes of these types are thought to have operated during the mid to late Miocene (<~15 Myr) to present near the Colorado plateau.

As an alternative, we suggest that foundering is driven by thermochemical convection (Fig. 4): adiabatically upwelling mantle generates buoyant basaltic partial melts that intrude the base and sides of the Colorado plateau lithosphere. Crystallization of such melts can destabilize the base of the lithosphere by refertilizing the pre-existing depleted mantle with basalt/eclogite/pyroxenite dykes or diffuse metasomatic zones²⁹. Peridotite xenoliths in Eocene minette dykes in the central Colorado plateau show such rejuvenation. These xenoliths define a geotherm that indicates a thermochemical boundary layer

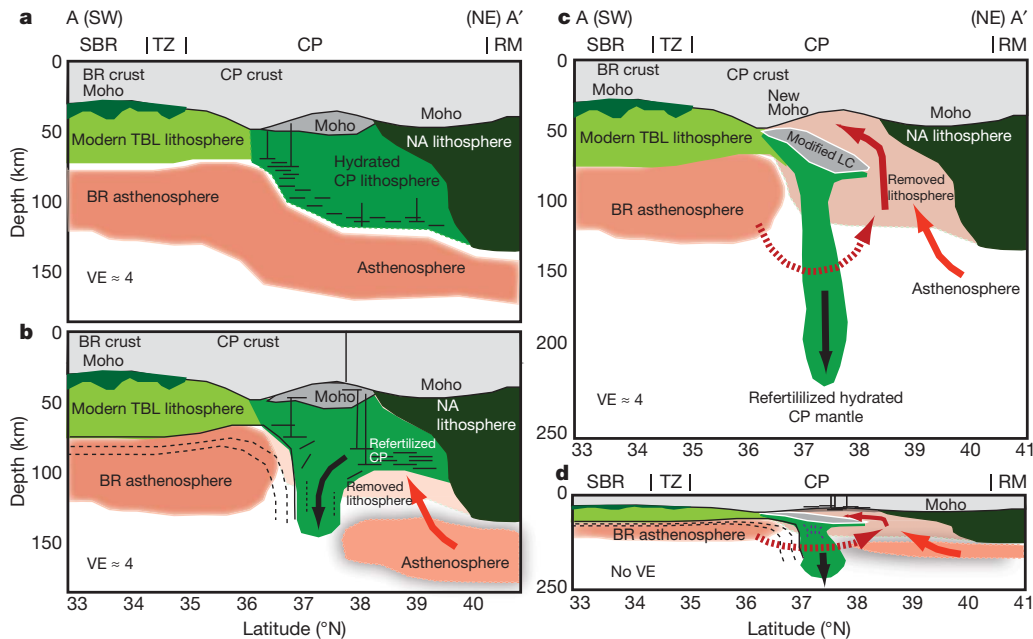


Figure 4 | The inferred progression of events associated with lithospheric foundering and the geometry of the drip today. **a**, The lithosphere and asthenosphere as they existed at some time following Farallon slab removal. The Colorado plateau lithosphere has been hydrated, and is being invaded by small-volume melts from the asthenosphere. The ~50 km of topography on the LAB along the southwestern edge of the Colorado plateau permits small-volume decompression melting. BR, Basin and Range; NA, North American lithosphere; TBL, thermal boundary layer. **b**, The small increase in density from freezing melts, schematically shown as solid back lines, and the viscosity reduction from hydration and advected heat, destabilizes the lithosphere and

thickness of ~120–150 km. The xenoliths show a compositional spectrum (in terms of Mg number, $Mg\# = \text{atomic Mg}/(\text{Mg} + \text{Fe})$) of 0.91–0.92—typical of depleted cratonic mantle—to values lower than the canonical value of ambient convecting mantle ($Mg\# = 0.89$)³⁰, suggesting that the base of the lithosphere may have been substantially refertilized. Refertilization leads to a small but important compositional density increase that can exceed the original positive buoyancy of depleted Colorado plateau cratonic mantle. Refertilization by melt infiltration also would have advected heat into the base of a North American lithosphere. Already hydrated by low-angle Farallon plate subduction, it would be further weakened thermally, reducing viscous resistance to the newly acquired negative buoyancy forces and thereby initiating foundering.

We suggest that such magmatism commenced with mantle return flow in response to late Eocene–early Miocene rollback or collapse of the flat-subducting Farallon plate. This period was characterized by an ignimbrite flare-up³¹, manifested in the formation of numerous laccoliths, plutons and porphyry copper deposits in western North America³². Any magma-induced destabilization mechanism is ultimately driven by the magmatic flux, which depends on the amount of ‘head-space’ for adiabatic upwelling of the underlying undepleted mantle, making the pre-existing and evolving topography of the LAB a primary control on such processes (Fig. 4). For example, thin lithosphere adjacent to thick lithosphere would facilitate generation of more magmas and hence be more prone to thermochemical destabilization. The thick lithosphere of the Colorado plateau was resistant to such destabilization, but was vulnerable to destabilization around its margins from the sides where it abuts thin, extended Basin and Range lithosphere. This thermochemical erosion will always initiate wherever the LAB rapidly shallows. As the drip progresses, more head-space is created for melt invasion and refertilization on its inboard side, further feeding the instability (Fig. 4). Ultimately, the entire thickness of lithospheric mantle is involved in the instability, which reaches the lower

crust: overall, the deeper foundering appears as a convective drip, but at the lower crust, which is relatively weak in comparison to the uppermost mantle, the downwelling takes the form of a delamination-like process, with deformation guided by the strength contrast between upper mantle and lower crust.

c, d, The drip as we infer it from the seismic data, shown at respectively 4:1 and 1:1 vertical exaggeration (VE). The re-fertilized Colorado plateau mantle has been removed almost completely, delaminating the lowermost crust with it. Asthenosphere is invading the region from beneath the drip (solid red arrows) and around the peripheries of the drip (dashed red arrow). We infer that the lowermost crust (LC) involved in the downwelling has been modified by intrusion of basaltic melts that froze to produce high density eclogites. In **a–d**, the range of latitude shown corresponds to ~1,000 km.

crust: overall, the deeper foundering appears as a convective drip, but at the lower crust, which is relatively weak in comparison to the uppermost mantle, the downwelling takes the form of a delamination-like process, with deformation guided by the strength contrast between upper mantle and lower crust.

We propose that a series of such events have been removing the lithosphere from the Colorado plateau peripheries since the Farallon slab was removed 20–30 Myr ago, and that we have imaged only the most recent of these. These events are responsible for the uneven, outside-in magmatic invasion of the plateau, as well as uplift of its edges and interior.

METHODS SUMMARY

Finite-frequency seismic body wave tomography is a standard means of including Fresnel zone effects in constructing a three-dimensional image of the Earth from teleseismic travel times. The finite-frequency Rayleigh wave tomography is a regional study of the Colorado plateau and its surroundings. This form of Rayleigh wave tomography gives absolute isotropic v_s measurements, and, because the waves travel horizontally, provides somewhat better vertical resolution of upper mantle v_s structure than teleseismic body wave tomography. Rayleigh waves in the band we examined (0.0067–0.05 Hz) are sensitive to v_s structure from the mid-crust, ~20 km depth, into the upper mantle, ~150–200 km depth.

Receiver function imaging is a means to make a scattered wave image of the subsurface using P to S (or S to P) converted waves, usually from teleseismic earthquake signals. The PdS receiver function is created by deconvolving the direct P wave recorded on the vertical component of motion from the radial component of motion. The deconvolution removes the earthquake source function, and replaces it with a known shaping pulse. The time difference between direct P and the scattered S waves on the receiver function, combined with the incidence angle of the P wave and an estimated velocity model, are used to back-project the receiver function in space to the points of conversion from P to S. Summing partial images for many earthquakes recorded by many stations improves the signal to noise ratio of the image. The process for making SdP receiver functions is similar. Direct teleseismic S waves have lower frequency (<0.2–0.1 Hz) content than the teleseismic P waves (<~2.0 Hz), and therefore produce a lower frequency image.

Full Methods and any associated references are available in the online version of the paper at www.nature.com/nature.

Received 16 July 2010; accepted 11 March 2011.

- Thompson, G. A. & Zoback, M. L. Regional geophysics of the Colorado Plateau. *Tectonophysics* **61**, 149–181 (1979).
- Schmandt, B. & Humphreys, E. D. Complex subduction and small-scale convection revealed by body-wave tomography of the western United States upper mantle. *Earth Planet. Sci. Lett.* **297**, 435–445 (2010).
- Humphreys, E. *et al.* How Laramide-age hydration of North American lithosphere by the Farallon slab controlled subsequent activity in the western United States. *Int. Geol. Rev.* **45**, 575–595 (2003).
- Lee, C.-T. A., Yin, Q., Rudnick, R. L. & Jacobsen, S. B. Preservation of ancient and fertile lithospheric mantle beneath the southwestern United States. *Nature* **411**, 69–73 (2001).
- Li, Z.-X. A., Lee, C.-T., Peslier, A. H., Lenardic, A. & Mackwell, S. J. Water contents in mantle xenoliths from the Colorado Plateau and vicinity: implications for the mantle rheology and hydration-induced thinning of continental lithosphere. *J. Geophys. Res.* **113**, B09210, doi:10.1029/2007JB005540 (2008).
- Roy, M., Jordan, T. H. & Pederson, J. Colorado Plateau magmatism and uplift by warming of heterogeneous lithosphere. *Nature* **459**, 978–982 (2009).
- Crow, R. S. *et al.* Shrinking of the Colorado Plateau via lithospheric mantle erosion: evidence from Nd and Sr isotopes and geochronology of Neogene basalts. *Geology* **39**, 27–30 (2011).
- Karlstrom, K. E., Crow, R., Crossey, L. J., Coblentz, D. & Van Wijk, J. W. Model for tectonically driven incision of the younger than 6 Ma Grand Canyon. *Geology* **36**, 835–838 (2008).
- Smith, D. Insights into the evolution of the uppermost continental mantle from xenolith localities on and near the Colorado Plateau and regional comparisons. *J. Geophys. Res.* **105**, 16769–16781 (2000).
- Livaccari, R. F. & Perry, F. V. Isotopic evidence for preservation of Cordilleran lithospheric mantle during the Sevier-Laramie orogeny, western United States. *Geology* **21**, 719–722 (1993).
- Humphreys, E. D. Post-Laramide removal of the Farallon slab, western United States. *Geology* **23**, 987–990 (1995).
- Huntington, K. W., Wernicke, B. P. & Eiler, J. M. Influence of climate change and uplift on Colorado Plateau paleotemperatures from carbonate clumped isotope thermometry. *Tectonics* **29**, TC3005, doi:10.1029/2009TC002449 (2010).
- Spencer, J. Uplift of the Colorado Plateau due to lithosphere attenuation during Laramide low-angle subduction. *J. Geophys. Res.* **101**, 13595–13609 (1996).
- Moucha, R. *et al.* Deep mantle forces and the uplift of the Colorado Plateau. *Geophys. Res. Lett.* **36**, L19310, doi:10.1029/2009GL039778 (2009).
- van Wijk, J. W. *et al.* Small-scale convection at the edge of the Colorado Plateau: implications for topography, magmatism, and evolution of Proterozoic lithosphere. *Geology* **38**, 611–614 (2010).
- Benz, H. M. & McCarthy, J. Evidence for an upper mantle low velocity zone beneath the southern Basin and Range – Colorado Plateau transition zone. *Geophys. Res. Lett.* **21**, 509–512 (1994).
- Henstock, T. J., Levander, A. & DeepProbe Working Group. Probing the Archean and Proterozoic lithosphere of western North America. *GSA Today* **8**, 1–5 16–17 (1998).
- Buehler, J. & Shearer, P. Pn tomography of the western United States using USArray. *J. Geophys. Res.* **115** B09315 (2010).
- Schmandt, B. & Humphreys, E. Complex subduction and small-scale convection revealed by body-wave tomography of the western United States upper mantle. *Earth Planet. Sci. Lett.* **297**, 435–445 (2010).
- Bassin, C., Laske, G. & Masters, G. The current limits of resolution for surface wave tomography in North America. *Eos* **81**, F897 (2000).
- Bird, P. Continental delamination and the Colorado Plateau. *J. Geophys. Res.* **84**, 7561–7571 (1979).
- Morency, C. & Doin, M.-P. Numerical simulations of the mantle lithosphere delamination. *J. Geophys. Res.* **109**, B03410, doi:10.1029/2003JB002414 (2004).
- Conrad, C. P. & Molnar, P. Convective instability of a boundary layer with temperature- and strain-rate-dependent viscosity in terms of 'available buoyancy'. *Geophys. J. Int.* **139**, 51–68 (1999).
- Bird, P. Laramide crustal thickening event in the Rocky Mountain foreland and Great Plains. *Tectonics* **3**, 741–758 (1984).
- Kay, S. M., Coira, B. & Viramonte, J. Young mafic back arc volcanic rocks as indicators of continental lithospheric delamination beneath the Argentine Puna Plateau, Central Andes. *J. Geophys. Res.* **99**, 24323–24339 (1994).
- Ducea, M. N. & Saleeby, J. B. Buoyancy sources for a large, unrooted mountain range, the Sierra Nevada, California; evidence from xenolith thermobarometry. *J. Geophys. Res.* **101**, 8229–8244 (1996).
- Bird, P. Formation of the Rocky Mountains, Western United States: a continuum computer model. *Science* **239**, 1507 (1988).
- Menzies, M., Xu, Y., Zhang, H. & Fan, W. Integration of geology, geophysics and geochemistry: a key to understanding the North China Craton. *Lithos* **96**, 1–21 (2007).
- Foley, S. F. *et al.* The composition of near-solidus melts of peridotite in the presence of CO₂ and H₂O between 40 and 60 kbar. *Lithos* **112**, 274–283 (2009).
- Ehrenberg, S. N. Petrogenesis of garnet Iherzolite and megacrystalline nodules from the Thumb, Navajo volcanic field. *J. Petrol.* **23**, 507–547 (1982).
- Lipman, P. W. in *The Cordilleran Orogen: Contemporaneous U. S.* (eds Burchfiel, B. C., Lipman, P. W. & Zoback, M. L.) 481–514 (Geological Society of America, 1992).
- Nelson, S. T., Davidson, J. P. & Sullivan, K. R. New age determinations of central Colorado Plateau Laccoliths, Utah — recognizing disturbed K-Ar systematics and re-evaluating tectonomagmatic relationships. *Geol. Soc. Am. Bull.* **104**, 1547–1560 (1992).

Supplementary Information is linked to the online version of the paper at www.nature.com/nature.

Acknowledgements The USArray data are from the IRIS DMS. A.L., K.L., M.S.M., E.D.H. and B.S. were supported by NSF EarthScope grants EAR-0844741, EAR-0844760 and EAR-0911006. Part of this research was initiated at the CIDER 2008 workshop (A.L., M.S.M.), and part was initiated at the GFZ-Potsdam (A.L.). A.L. acknowledges an Alexander von Humboldt Foundation Research Prize.

Author Contributions A.L. wrote the receiver function analysis codes and processed the PdS receiver functions. B.S. and E.D.H. wrote the tomography codes and processed the body wave data. M.S.M. and A.L. analysed the SdP receiver functions. K.L. analysed the Rayleigh wave data. K.E.K. and R.S.C. provided uplift and geochemical information. C.-T.A.L. provided geochemical information. All the authors participated in the interpretation.

Author Information Reprints and permissions information is available at www.nature.com/reprints. The authors declare no competing financial interests. Readers are welcome to comment on the online version of this article at www.nature.com/nature. Correspondence and requests for materials should be addressed to A.L. (alan@rice.edu).

METHODS

The finite-frequency body wave tomography is described in a study of southern California³³. Finite-frequency seismic body wave tomography is a standard means of including Fresnel zone effects in constructing a three-dimensional image of the Earth from teleseismic travel times². The finite-frequency Rayleigh wave tomography is a regional study of the Colorado plateau³⁴ and its surroundings, calculated with the two-plane wave method³⁵. This form of Rayleigh wave tomography gives absolute isotropic v_S measurements, and, because the waves travel horizontally, provides somewhat better vertical resolution of upper-mantle v_S structure than teleseismic body wave tomography. Rayleigh waves in the band we examined (0.0067–0.05 Hz) are sensitive to v_S structure from the mid-crust (~20 km) into the upper mantle (~150–200 km depth). Rayleigh waves are insensitive to v_P and density structure at these depths.

Receiver function imaging is a means to make a scattered wave image of the subsurface using P to S (or S to P) converted waves^{36,37}, usually from earthquake signals. The Ps receiver function is created by deconvolving the direct P wave on the vertical (or rotated longitudinal) component of motion from the radial (or rotated S) component and the tangential component. The deconvolution removes the earthquake source function and replaces it with a known shaping pulse. The time difference between direct P and the scattered S waves on the receiver function (or direct S and scattered P), combined with a known or estimated incidence angle and back-azimuth of the P-wave, can be used to back-project the receiver function laterally and in depth to the point of conversion from P to S. The back projection

requires an estimate of the P and S velocity fields. Summing many partial images from receiver functions recorded at many seismograph stations for many earthquakes, a process called common conversion point (CCP) stacking³⁸, improves the signal to noise ratio of the image. For Ps receiver functions, earthquakes between ~40° and 90° from the seismograph station are used. The process for making SdP receiver functions is similar³⁷: The direct S arrival is deconvolved from the longitudinal component to isolate scattered P waves. Earthquakes between 55° and 85° from the seismograph station are used. The direct teleseismic S waves have lower frequency (<0.2–0.1 Hz) content than the teleseismic P waves (<~2.0 Hz) owing to higher attenuation in the Earth, and therefore produce a lower frequency image.

33. Schmandt, B. & Humphreys, E. Seismic heterogeneity and small-scale convection in the southern California upper mantle. *Geochem. Geophys. Geosyst.* **11**, Q05004, doi:10.1029/2010GC003042 (2010).
34. Liu, K., Levander, A., Niu, F. & Miller, M. S. Imaging crustal and upper mantle structure beneath the Colorado Plateau using finite-frequency Rayleigh wave tomography. *Geochem. Geophys. Geosyst.* (submitted).
35. Forsyth, D. W. & Li, A. in *Seismic Earth: Array Analysis of Broadband Seismograms* Vol. 157 (eds Levander, A. & Nolet, G.) 81–97 (American Geophysical Union, 2005).
36. Langston, C. A. Corvallis, Oregon, crustal and upper mantle receiver structure from teleseismic P and S waves. *Bull. Seismol. Soc. Am.* **67**, 713–724 (1977).
37. Yuan, X., Kind, R., Li, X. & Wang, R. The S receiver functions: synthetics and data example. *Geophys. J. Int.* **165**, 555–564 (2006).
38. Dueker, K. G. & Sheehan, A. F. Mantle discontinuity structure from midpoint stacks of converted P to S waves across the Yellowstone hotspot track. *J. Geophys. Res.* **102**, 8313–8327 (1997).